Interplay of alternation and further neighbor interaction in $S = \frac{1}{2}$ spin chains: A case study of $Cs_2CuAl_4O_8$

Badiur Rahaman,[1] Satyaki Kar,[2] Alexandre Vasiliev,[3,4,5] and Tanusri Saha-Dasgupta[6,7]

[1]*Department of Physics, Aliah University, Kolkata 700156, India*
[2]*Department of Theoretical Physics, Indian Association for the Cultivation of Science, Kolkata 700032, India*
[3]*Department of Low Temperature Physics and Superconductivity, Lomonosov Moscow State University, Moscow 119991, Russia*
[4]*Department of Theoretical Physics and Quantum Technology, National University of Science and Technology MISiS, Moscow 119049, Russia*
[5]*Functional Materials Laboratory, National Research South Ural State University, Chelyabinsk 454080, Russia*
[6]*Center for Mathematical, Computational and Data Science, Indian Association for the Cultivation of Science, Kolkata 700032, India*
[7]*Department of Condensed Matter Physics and Materials Science, S. N. Bose National Centre for Basic Sciences, Kolkata 700106, India*

Using Wannier function formulation and total energy calculations by first-principles density functional theory (DFT), we derive the underlying spin model of a recently synthesized compound, $Cs_2CuAl_4O_8$, having zeolitelike network structure. The computed magnetic interactions show that the interchain Cu-Cu interactions are negligibly small compared to intrachain Cu-Cu interactions, thus characterizing $Cs_2CuAl_4O_8$ as a prototypical one-dimensional (1D) spin-$\frac{1}{2}$ system. Interestingly, the DFT-derived 1D spin model features a combination of alternating ferromagnetic-antiferromagnetic interactions, together with the presence of both nearest- and next-nearest-neighbor interactions, making it an unprecedented case. The solution of the derived spin model of the compound using the quantum Monte Carlo technique shows reasonably good agreement with the experimental susceptibility data, measured in the presence of the magnetic field. The presence of spin gap is suggested by quantum Monte Carlo simulations in the zero-field condition, which is cross-checked by a more rigorous exact diagonalization study. Motivated by the intricacy of the derived spin model, we further examine the ground-state properties of this model in the parameter space of exchange interactions, which shows the possibility of driving quantum phase transition between gapped and gapless spin excitation. Our study is expected to shed light on the fascinating world of 1D quantum spin systems.

I. INTRODUCTION

Low-dimensional quantum spin systems offer rich physics due to the dominance of the quantum fluctuation effect. One-dimensional (1D) and two-dimensional $S = 1/2$ or $S = 1$ systems like chain compounds [1], odd- and even-leg ladders [2,3], tubular systems [4], and kagome, honeycomb, and triangular layers [5–7] have received sustained attention over the years due to the importance of the quantum effect arising due to the reduced dimensionality and smallness of the spin value. The ground state of prototype 1D systems exhibiting low-dimensional quantum magnetism with uniform antiferromagnetic (AFM) Heisenberg interaction [8] can be gapless ($S = 1/2$) or gapped ($S = 1$), depending on the spin value [9,10]. Starting from the gapless spectrum of the uniform AFM Heisenberg $S = 1/2$ chain, the gapped solution with a singlet ground state and triplet excited state can be obtained by alternating the nearest-neighbor intrachain exchange interaction parameter [11] between J and J'. Alternatively, gap can appear in a uniform $S = 1/2$ chain with both nearest (J) and next-nearest (J_{nnn}) exchange interactions for $J_{nnn}/J > 0.25$ [12]. It is of interest to explore the combined effect of J-J' alternation and J-J_{nnn} competition in a 1D spin-chain model. For this purpose, one must identify a compound which shows (i) heavily suppressed interchain interactions to exclude formation of three-dimensional magnetic order and (ii) the

presence of both alternating nearest-neighbor exchange and significant next-nearest-neighbor exchange.

The recently synthesized [13] dicesium copper tetra-aluminate compound, $Cs_2CuAl_4O_8$, appears to be a probable candidate in this respect due to its zeolitelike structure containing well-separated edge-sharing chains of Cu^{2+} ions in square oxygen coordination. The magnetic susceptibility of the synthesized compound was measured [13], and from the fit of the temperature dependence of the susceptibility, it was concluded that this compound belongs to the category of spin-chain compounds, which requires a description beyond the uniform chain model. The simple fitting treatment adapted in Ref. [13] makes it hard to predict any further details, which would involve prediction of exchange paths and the relative magnitudes of various magnetic interactions.

The first-principles modeling of materials, which takes into account the chemistry and structural information accurately, turns out to be a useful tool in this context. This approach has been immensely successful in the modeling of various different spin compounds [14]. In this study, considering the case of $Cs_2CuAl_4O_8$, through first-principles calculations we establish that $Cs_2CuAl_4O_8$ satisfies both conditions (i) and (ii), thereby representing the situation of a 1D spin chain with alternating nearest-neighbor as well as appreciable next-nearest-neighbor exchanges. The underlying spin model turns out to be rather interesting in several ways. First, we find

144412-1

the next-nearest-neighbor exchange is about three times larger in magnitude than the nearest-neighbor exchanges, which is counterintuitive. We rationalize this situation in terms of overlap of effective orbitals at the magnetic Cu site. Second, the two nearest-neighbor Cu-Cu exchanges are found to differ in sign, resulting in a spin chain having both AFM and ferromagnetic (FM) exchanges. We carry out a quantum Monte Carlo (QMC) study of the first-principles-derived spin model of $Cs_2CuAl_4O_8$ within the stochastic series expansion (SSE) implementation of QMC to compute the temperature-dependent magnetic susceptibility, which shows reasonable agreement with the experimental data, measured in the presence of field. The calculated zero-field magnetic susceptibility without consideration of the impurity effect suggests the ground state is gapped. This suggestion has been validated through a more rigorous exact diagonalization study of the spin spectrum by measuring the gap between the ground state and the first excited state and by carrying out a finite-size scaling analysis using a modified Lanczos technique. We further explore the J-J'-J_{nnn} parameter space and find that by suitable tuning of competing magnetic exchanges, the gapped solution can be converted to a gapless one, thereby driving a quantum phase transition.

II. $Cs_2CuAl_4O_8$

A. Crystal structure

$Cs_2CuAl_4O_8$ occurs in monoclinic symmetry with space group $P2_1/c$ with 6 f.u. in the unit cell. The basic magnetic units in the structure are regular and distorted squares of $Cu1O_4$ and $Cu2O_4$, respectively formed by two inequivalent Cu atoms, Cu1 and Cu2, surrounded by four O atoms in square coordinations, as shown in Fig. 1(a). The Cu1-O bond lengths are uniform (1.92 Å), while the Cu2-O bond lengths range from 1.89 to 1.93 Å, with an average value of 1.91 Å. The regular $Cu1O_4$ and distorted $Cu2O_4$ squares share a common edge and form the chain structure of magnetic ions, ···Cu1-Cu2-Cu2-Cu1···, running along the crystallographic a axis, as shown in Fig. 1(b). The edge-shared angles, as marked in Fig. 1(b), are $\theta_3 = 95.7°$ for Cu2-Cu2 and $\theta_1 = 94.0°$ and $\theta_2 = 95.1°$ for Cu1-Cu2. The ···Cu1-Cu2-Cu2-Cu1··· spin chains are connected to each other through AlO_4 tetrahedral units. Cs ions occupy the voids and channels in the Cu1-Cu2-Al-O zeolitelike three-dimensional (3D) network to give cohesion to the structure, as shown in Fig. 1(c).

B. Electronic structure

In order to gain microscopic understanding of the electronic behavior of $Cs_2CuAl_4O_8$ we perform first-principles density functional theory (DFT) calculations [15] within the generalized gradient approximation (GGA) [16] for the exchange-correlation functional following the Perdew-Burke-Ernzerhof prescription [16]. Calculations are carried out in the plane-wave basis as implemented within the Vienna Ab initio Simulation Package (VASP) [17] as well as in the Nth-order muffin-tin orbital (NMTO) [18] and linear muffin-tin orbital (LMTO) [19] basis sets as implemented in the STUTTGART code. The consistency between the two sets of calculations
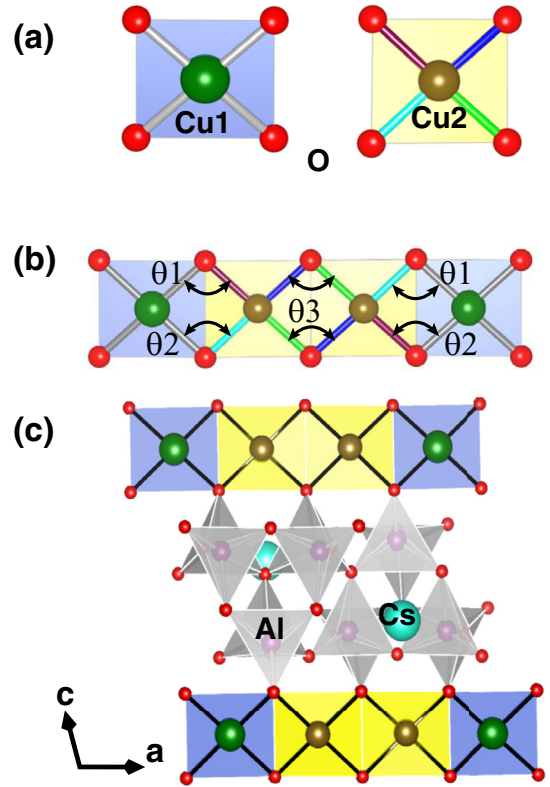

FIG. 1. Crystal structure of $Cs_2CuAl_4O_8$. (a) The basic structural units, $Cu1O_4$ and $Cu2O_4$, containing the magnetic Cu^{2+} ion. (b) The 1D chain formed by edge-shared $Cu1O_4$ and $Cu2O_4$ square units. (c) The 3D structure formed by ···Cu1-Cu2-Cu2-Cu1··· chains connected by AlO_4 units. The Cs^{1+} ions occupy the voids and channels. The green, brown, red, gray, and cyan balls represent Cu1, Cu2, O, Al, and Cs atoms, respectively.

in two choices of basis sets is cross-checked in terms of band structure, density of states, magnetic moments, etc.

For the self-consistent electronic structure calculation in the LMTO basis, the basis set is chosen to be Cu sd, Cs sp, Al sp, and O sp. Thirty different classes of empty spheres have been used to space fill the system. The self-consistency is achieved by using 64 k points in the irreducible Brillouin zone. The NMTO method, which relies on the self-consistent potential generated by the LMTO method, is used for deriving the massively downfolded, low-energy Hamiltonian defined in the basis of effective Cu $d_{x^2-y^2}$ Wannier functions as well as the only Cu d Hamiltonian by integrating out all the degrees of freedom, except Cu $d_{x^2-y^2}$ in the former and all but Cu d in the latter case. The on-site element of the real-space representation of the only Cu d Hamiltonian provides information about the crystal field splitting at the Cu sites, while the off-site elements of the massively downfolded, low-energy Hamiltonian provide information about effective hopping interactions between the magnetic sites, which are related to magnetic exchange. The energetically accurate plane-wave basis set calculations are employed to calculate the total energy of different configurations of Cu spins to derive the magnetic exchanges from the total energy consideration. For the self-consistent field calculations in the plane-wave basis,
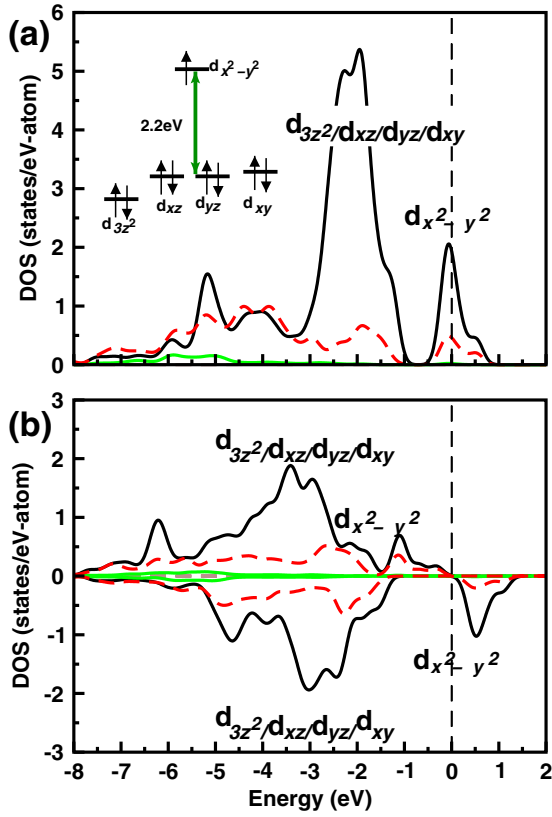
FIG. 2. (a) Non-spin-polarized density of states (DOS) of $Cs_2CuAl_4O_8$, projected onto Cu d (black solid line), O p (red dashed line), As p (green solid line), and Cs s (brown dashed line), plotted as a function of energy. The zero of the energy is fixed at the GGA Fermi energy. (b) The same as in (a), but shown for the spin-polarized calculation. The inset in (a) shows the crystal field splitting at the Cu site. The average picture of Cu1 and Cu2 is shown, as the difference between the two turned out to be small, both in DOS and in crystal field splitting.

an energy cutoff of 450 eV and a $4 \times 4 \times 2$ Monkhorst-Pack k-point mesh are found to provide a good convergence of the total energy with a tolerance limit of 10^{-5} eV. In the total energy calculations, the missing correlation energy at Cu sites beyond GGA is considered in terms of GGA calculations supplemented with Hubbard U correction (GGA+U) [20], with a choice of $U = 7$ eV and $J_H = 0.9$ eV for Cu sites.

The calculated non-spin-polarized density of states within the GGA scheme of calculation, projected onto Cu d, O p, Al p, and Cs s, is shown in Fig. 2(a). The inset shows the crystal field splitting at the Cu sites, as given by the on-site matrix element of the only Cu d real-space Hamiltonian, obtained through the NMTO-downfolding technique. The square environment of oxygen atoms surrounding Cu splits the d states of Cu into low-lying closely spaced $d_{3z^2-r^2}$, d_{xz}, d_{yz}, d_{xy} and a high-lying $d_{x^2-y^2}$ state, which is separated from the rest by a large crystal field splitting of ≈ 2.2 eV. This results in a half-filled Cu $d_{x^2-y^2}$ state of Cu1^{2+} and Cu2^{2+} ions, strongly admixed with O p states, crossing the Fermi level. Considering the nominal valences of Cu and oxygen as 2+ and 2−, respectively, the oxidation states of Cs and Al are set as +1 and +3, respectively. This gives rise to the filled-shell

TABLE I. Calculated magnetic moment at different atomic sites of $Cs_2CuAl_4O_8$.

Atom	Magnetic moment (units of μ_B)
Cu1	0.707
Cu2	0.709
O	0.129
Al	0.005
Cs	0.001

[Ar] configuration for Al and [Xe] configuration for Cs, with empty Al p and Cs s valence states.

While the non-spin-polarized calculation results in a metallic solution, consideration of spin polarization results in an insulating solution, with a filled Cu $d_{x^2-y^2}$ state in the majority-spin channel and an empty Cu $d_{x^2-y^2}$ state in the minority-spin channel, as shown in Fig. 2(b). The calculated magnetic moments at two inequivalent Cu sites, the average moment at the oxygen site, and those at the Al and Cs sites are shown in Table I. The magnetic moment at the O site is found to be unusually large, in contrast to the generally believed nonmagnetic character of oxygen. This reflects the strong Cu-O covalency which contributes to the superexchange path connecting two Cu sites. The magnetic moments at Cs and Al sites are found to be tiny, indicating their closed-shell configurations and little covalency with Cu. The total magnetic moment is found to be $1\mu_B$/f.u., corresponding to one Cu^{2+} ion in the formula unit.

C. Magnetic exchanges

In order to identify the dominant effective Cu-Cu interactions present in the compound, the massive downfolding technique of NMTO is applied. This amounts to the construction of effective Cu $d_{x^2-y^2}$ Wannier functions starting from the full DFT electronic structure by keeping active only the Cu $d_{x^2-y^2}$ degrees of freedom and downfolding the rest of the degrees of freedom associated with O, Al, Cs, and other Cu d orbitals. This procedure takes into account the renormalization of Cu $d_{x^2-y^2}$ orbitals due to finite hybridization with other degrees of freedom, especially with O p. The off-diagonal terms of the real-space Hamiltonian defined in the basis of the effective Cu $d_{x^2-y^2}$ Wannier function provide estimates of various effective Cu-Cu hopping interactions.

The dominant effective Cu-Cu hopping interactions within the Cu chain turned out to consist of two nearest-neighbor (NN) hoppings (t and t') and two next-nearest-neighbor (NNN) hoppings (t_{nnn} and t'_{nnn}), as shown in Fig. 3(a). The values of these hopping integrals, as given by the NMTO-downfolding calculation, are found to be $t = 62.6$ meV, $t' = 78.3$ meV, $t_{nnn} = 126.5$ meV, and $t'_{nnn} = 119.7$ meV. The interchain Cu-Cu hoppings turn out to be significantly smaller than intrachain hoppings, establishing the one-dimensionality of the compound. The NN hoppings t and t' are mediated by Cu1 $d_{x^2-y^2}$-O p-Cu2 $d_{x^2-y^2}$ and Cu2 $d_{x^2-y^2}$-O p-Cu2 $d_{x^2-y^2}$ superexchange paths, while the NNN hoppings t_{nnn} and t'_{nnn} are mediated by Cu2 $d_{x^2-y^2}$-O p-Cu1 $d_{x^2-y^2}$-O p-Cu2 $d_{x^2-y^2}$ and Cu1 $d_{x^2-y^2}$-O p-Cu2 $d_{x^2-y^2}$-O p-Cu2 $d_{x^2-y^2}$
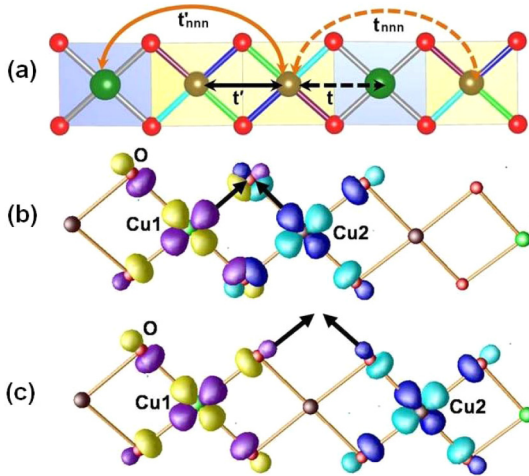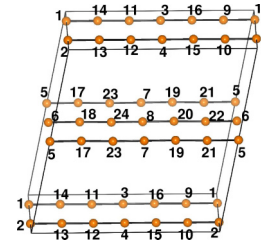
FIG. 3. (a) The dominant effective Cu-Cu hopping interactions, as given by NMTO-downfolding calculations. The color convention of atoms is the same as in Fig. 1. (b) Overlap of effective Cu $d_{x^2-y^2}$ Wannier functions placed at nearest-neighbor Cu sites in the chain. (c) The same as in (b), but plotted for Wannier functions placed at next-nearest-neighbor Cu sites in the chain. Plotted are the orbital shapes (constant-amplitude surfaces) with lobes with opposite signs colored differently.

	1	2	3–8	9	10	11	12	13	14	15	16–24	Δ E
FM	+	+	+	+	+	+	+	+	+	+	+	0
AFM1	−	+	+	+	+	+	+	+	+	+	+	−09.350
AFM2	+	+	+	+	−	+	−	+	+	+	+	−16.230
AFM3	−	−	+	−	−	+	+	+	+	+	+	−21.790
AFM4	+	+	+	+	−	+	+	+	−	+	+	−24.841
AFM5	+	+	+	+	−	+	−	+	−	+	+	−48.906

FIG. 4. Different magnetic configurations of the Cu ions in the supercell, used to determine the magnetic interactions. The numbering of the Cu ions, as indicated in the table, are as shown in the diagram. The last column gives the relative GGA+U energies (in meV).

supersuperexchange paths, respectively. It is interesting to note that the NNN Cu1-Cu2 and Cu2-Cu2 hoppings mediated by the supersuperexchange path are significantly stronger (by a factor of about 1.5–2) than the NN Cu1-Cu2 and Cu2-Cu2 hoppings mediated by the nearest-neighbor superexchange path, although the corresponding Cu-Cu distances are significantly longer for NNN (by a factor of about 2) than that for NN. To have a microscopic understanding of this curious situation, we consider the overlap of effective Cu $d_{x^2-y^2}$ Wannier functions placed at nearest-neighbor and next-nearest-neighbor Cu sites, as shown in Figs. 3(b) and 3(c), respectively. While the central part of these effective Wannier functions are shaped according to $d_{x^2-y^2}$ symmetry, the tails sitting at the neighboring oxygen sites are shaped according to O p_x or O p_y symmetries, indicating the formation of strong $pd\sigma$ antibonds. For Wannier functions placed at neighboring Cu sites, the overlap of the tails of the two functions at the common edge-shared oxygen positions is found to be almost orthogonal, thereby significantly weakening the effective NN hopping. On the other hand, for the Wannier functions placed at NNN Cu sites, the tails at O sites of the two functions point towards each other (marked by arrows in Fig. 3), indicating stronger overlap of the two functions. The above analysis thus rationalizes the counterintuitive numerical estimates of the hoppings.

The NMTO-downfolding analysis which helps us to identify the nature of the underlying exchange network establishes that magnetic properties of $Cs_2CuAl_4O_8$ should be described by a 1D J-J'-J_{nnn}-J'_{nnn} spin model, where J, J', J_{nnn}, and J'_{nnn} denote the magnetic exchanges corresponding to hopping interactions t, t', t_{nnn}, and t'_{nnn}, respectively. Magnetic exchanges J can be obtained from the knowledge of hopping interactions t using the superexchange formula $J = 4t^2/U$,

where U is the on-site Hubbard interaction. However, this approach, being perturbative in nature, is approximate and provides information about only the antiferromagnetic contributions. The presence of superexchange paths, involving Cu-O-Cu bond angles close to 90°, in the discussed compound makes the consideration of the ferromagnetic contribution to magnetic exchange necessary. Therefore in order to obtain a quantitative measure of magnetic interactions corresponding to NMTO-downfolding-identified dominant Cu-Cu hoppings, we perform total energy calculations of different configurations of Cu^{2+} spins in a supercell of $2 \times 2 \times 1$ dimensions and extract the magnetic exchanges by mapping the calculated DFT energies to that of a Heisenberg model (refer to Fig. 4 for the considered configurations and the energetic). We consider various independent combinations of four different energy differences listed in Fig. 4 in order to avoid any dependency on the chosen spin configurations. Following this, we obtain $J = -2.22 \pm 0.20$ meV, $J' = 2.30 \pm 0.52$ meV, $J_{nnn} = 7.01 \pm 0.39$ meV, and $J'_{nnn} = 6.85 \pm 0.13$ meV. The positive (negative) signs of interactions indicate antiferromagnetic (ferromagnetic) exchange interactions. It is important to note here the two alternating exchange interactions, J and J', involve two different nearest-neighbor edge-sharing interactions, one between $Cu1O_4$ and $Cu2O_4$ and another between $Cu2O_4$ and $Cu2O_4$. While the average Cu-O bond lengths involved in the two cases are the same (1.915 Å), it is the difference in the involved Cu-O-Cu bond angles in the two cases that is responsible for the alternation. In the case of the $Cu1O_4$-$Cu2O_4$ interaction (J) the involved bond angles are 94° and 95°, while in the case of the $Cu2O_4$-$Cu2O_4$ interaction (J') the involved bond angles are both 96°. We note that the involved bond angles in both cases are close to the borderline value of 90° for transition from an antiferromagnetic to ferromagnetic nature of interaction. However, the bond angles for $Cu1O_4$-$Cu2O_4$ interaction are closer to 90° than that for

the Cu2O4-Cu2O4 interaction. This makes J ferromagnetic and J' antiferromagnetic, although the magnitudes of both J and J' are about a factor of 3–3.5 smaller than the next-nearest-neighbor interactions, J_{nnn} and J'_{nnn}.

D. Magnetic susceptibility

DFT calculations indicate that both alternation and far-neighbor interactions are operative in $Cs_2CuAl_4O_8$. These calculations further reveal that the leading exchange interactions are the next-nearest-neighbor interactions, rather than nearest-neighbor interactions, although the NNN interactions are longer ranged than NN interactions. Additionally, NN interactions are positive as well as negative. This is expected to provide a strongly interacting system with several competing interactions, which can be modeled in terms of a $S = 1/2$ J-J'-J_{nnn}-J'_{nnn} spin-chain Hamiltonian, as given by

$$
H = J \sum_i^{N/3} [S_{3i-1} S_{3i-2} + S_{3i} S_{3i-1}] + J' \sum_i^{N/3} S_{3i} S_{3i+1}
$$
$$
+ J_{nnn} \sum_i^{N/3} S_{3i} S_{3i-2} + J'_{nnn} \sum_i^{N/3} [S_{3i+1} S_{3i-1} + S_{3i} S_{3i+2}],
$$
(1)

where i represents the position of the Cu site in the chain.

Considering a pure alternating chain model together with a Curie impurity term, the fit to experimentally measured temperature dependence of susceptibility provided a Landé g factor value of 2.32 and a value of the strongest exchange interaction parameter J of 63.7 K [14]. This simple fitting procedure, however, is unable to provide any microscopic details, nor does it provide a unique description. In fact, the insensitivity of susceptibility to the details of the spin model is well known. An excellent example in this case is that of $(VO)_2P_2O_7$, which was originally thought to be a candidate for a two-leg ladder based on the susceptibility fit [21]; a later extensive neutron study established it to be an alternating chain [22]. Thus in order to have a realistic description of the situation in $Cs_2CuAl_4O_8$, we consider the spin Hamiltonian, as given in Eq. (1), and the numerical solution of the problem is obtained employing the SSE technique of the QMC simulation, carried out on a chain of size $L = 96$. We set J'_{nnn}/J_{nnn} to 1, following the DFT estimate of 0.98. We note that the DFT-derived spin Hamiltonian consisting of nearest- and next-nearest-neighbor AFM interactions, as given in Eq. (1), is frustrated. As is well known, while QMC provides one of the powerful numerical approaches, its application to frustrated quantum spin models becomes severely restricted by the sign problem. A standard SSE-QMC simulation of this Hamiltonian would make the obtained results unreliable, unless one uses sophisticated tricks like defining a composite-spin system out of the original single-site basis, which may make the spin problem milder [23]. We have thus used an approximated Hamiltonian, which is expected to show a reduced frustration effect, providing more trustworthy results. This is described in Appendix A.

The theoretically calculated spin susceptibility can be related to experimentally measured molar susceptibility as $\chi = 0.375 S(S+1) g^2 \chi_{th}/J_{max}$, where $\chi_{th} = J_{max}/$

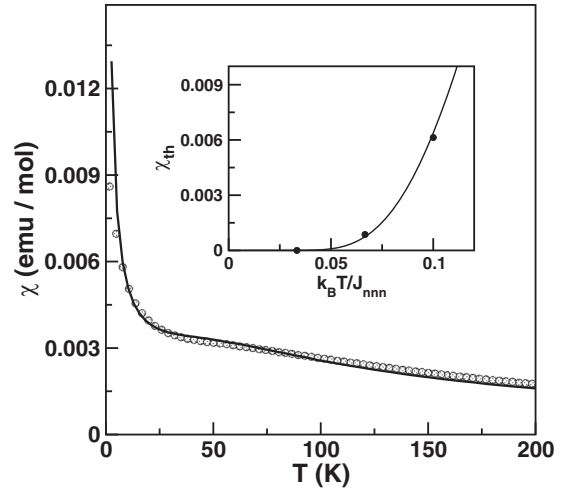FIG. 5. Temperature dependence of magnetic susceptibility for the $Cs_2CuAl_4O_8$ compound. The symbols correspond to experimental data [14], and the solid line corresponds to QMC-calculated susceptibility in the first-principles-derived J-J'-J_{nnn}-J'_{nnn} spin model in the presence of a magnetic field of 5 T. The inset shows the plot of χ_{th} without the impurity contribution calculated at zero magnetic field.

$k_B T \langle S_z^2 - \langle S_z \rangle^2 \rangle$, with J_{max} being the strongest coupling present. The comparison between the theoretically calculated susceptibility, after adding the impurity contribution of the form C/T, and the experimentally measured susceptibility at a magnetic field of 5 T is shown in Fig. 5. A fair match between the two was obtained for a Landé g factor value of $g = 2.25$, and the most dominant interaction of the J-J'-J_{nnn}-J'_{nnn} model was $J_{nnn} = 78$ K and $J/J_{nnn} = 0.33$. Both J_{nnn} and J_{nn}/J_{nnn} are found to be rather close to the DFT-estimated values of $J_{nnn} = 81$ K and $J/J_{nnn} = 0.32$. Repeating the calculation at zero magnetic field and following the low-temperature behavior of susceptibility appear to support the presence of a spin gap with a value of $0.04 J_{nnn}$, which amounts to about 3 K (see the inset in Fig. 5). While the use of the Hamiltonian presented in Appendix A provides reasonable results at high to moderate temperatures, for confirmation of the spin gap, which is the rather low temperature behavior, we rely more on the exact diagonalization and the Lanczos analysis for finite-size scaling presented in the next section.

III. EXACT DIAGONALIZATION RESULTS ON SPIN GAP

It is worth checking for the possible presence of spin gap in the discussed compound, with a more rigorous exact diagonalization study, due to the difficulties of the QMC simulation in the frustrated system mentioned above. Furthermore, the underlying spin model provides an interesting scenario, which is worthy of investigation from a model perspective that combines the alternating chain model with a competing nearest-neighbor–next-nearest-neighbor model. In particular, it will be worthwhile to investigate the influence of the variation of magnetic exchanges on the value of spin gap. For this purpose, we carry out an exact diagonalization calculation of a spin chain of length $L = 12$ within the setup of the periodic boundary condition. As in QMC calculations, we
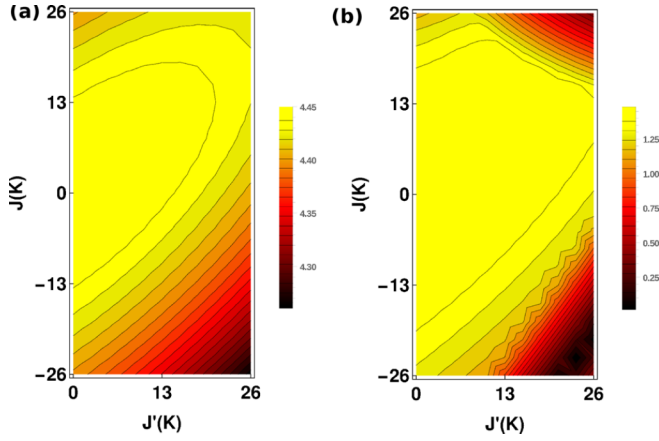
FIG. 6. Lowest-energy gap in the J-$J^{'}$ plane for the J-$J^{'}$-J_{nnn} chain model for (a) $J_{nnn} = 78$ K and (b) $J_{nnn} = 26$ K.

assume $J^{'}_{nnn} = J_{nnn}$. Fixing the value of dominant exchange J_{nnn} at 78 K, a value specific to $Cs_2CuAl_4O_8$, we vary the value of J and $J^{'}$ over a wide range. Specifically, the NN magnetic exchange J is varied from FM to AFM. The calculated spin gap as a function of J and $J^{'}$, measured as the gap between the ground state and lowest excited state, is shown in Fig. 6(a). We find the solution to be gapped in all cases and the gap value to be rather insensitive to the variation of J and $J^{'}$ as long as $J_{nnn} \gg |J|$. Interestingly, fixing $J/J^{'}$ to the DFT estimate of -0.97 gives a gap value of about 4 K, somewhat close to the value of 3 K obtained from the QMC calculation. A pertinent issue in the above conclusion is the effect of the finite-size lattice. Needless to say, a finite-size scaling analysis is required to deduce the spin-gap value at the limit of infinite length. Since the exact diagonalization calculation turned out to be prohibitively expensive for system sizes larger than 12, we have carried out further calculations using a modified Lanczos technique, the results of which are presented in Appendix B. The finite-size scaling done on the basis of additional calculations on a larger-sized lattice led us to conclude that for the realistic values of J, $J^{'}$, and J_{nnn} valid for the discussed compound, the spin-gap value is indeed close to 3–4 K. A dramatic change happens when reducing the J_{nnn} value and making it comparable to J. Figure 6(b) shows the same plot as Fig. 6(a), but for the choice of $J_{nnn} = 26$ K. We find this reduces the gap value drastically, with the maximum of the gap value in the J-$J^{'}$ plane being reduced by a factor of 3 or so. For competing values of $|J|$ and $J^{'}$, with the ferromagnetic nature of J, it might even be possible to drive the solution gapless, as seen from the plot presented in Fig. 6(b).

IV. SUMMARY AND OUTLOOK

To summarize, we have investigated the underlying spin model of $Cs_2CuAl_4O_8$, which is a recently synthesized compound with a phase containing both copper and a large alkali metal that exhibits a zeolitelike framework [13]. The measured magnetic susceptibility [13] shows the presence of a broad humplike feature signaling the low dimensionality of the underlying spin model [24]. However, in the absence of any detailed microscopic investigation, the pre-

cise nature of the magnetic model was hard to predict. Our first-principles calculation reveals an intriguing situation, which turned out to be a combination of an alternating spin-chain model and the competing nearest-neighbor–next-nearest-neighbor model, the latter in a specific limiting case being the celebrated Majumdar-Ghosh model [12]. Interestingly, the sign of the alternation parameter turns out to be negative, giving rise to the presence of both ferromagnetic and antiferromagnetic nearest-neighbor exchanges, making the model more intricate. The solution of this first-principles spin model derived using the quantum Monte Carlo technique provides a reasonable description of the experimentally measured magnetic susceptibility. The curious nature of the derived spin model prompts us to investigate the model further in parameter space. In particular, we explore the ground-state behavior of the model using an exact diagonalization technique in the parameter space of the alternation and the ratio of NNN to NN magnetic exchange. Our study shows a quantum phase transition from a gapful to gapless situation may possibly be triggered by tuning the value of the J_{nnn} interaction along with competing J and $J^{'}$. Experimentally, this may be achieved through biaxial straining by putting the thin film of the compound on a piezoelectric substrate, which along with bond lengths is also expected to tune the bond angles. We hope that our study will stimulate further activity on this exciting class of spin-chain systems with an interplay of alternation and far-neighbor interactions.

APPENDIX A: SPIN HAMILTONIAN FOR THE QMC CALCULATION

Setting $J_{nnn} = J^{'}_{nnn}$ and rewriting the spin-spin interaction term, as a combination of z-z and spin-raising/-lowering interactions, the spin Hamiltonian, as given in Eq. (1), becomes

$$H = J \sum_i^{N/3} \left[\left\{ S_{3i-1}^z S_{3i-2}^z + \frac{1}{2}(S_{3i-1}^+ S_{3i-2}^- + \text{H.c.}) \right\} \right.$$
$$\left. + \left\{ S_{3i}^z S_{3i-1}^z + \frac{1}{2}(S_{3i}^+ S_{3i-1}^- + \text{H.c.}) \right\} \right]$$
$$+ J^{'} \sum_i^{N/3} \left\{ S_{3i}^z S_{3i+1}^z + \frac{1}{2}(S_{3i}^+ S_{3i+1}^- + \text{H.c.}) \right\}$$
$$+ J_{nnn} \sum_i^{N} \left\{ S_i^z S_{i+2}^z + \frac{1}{2}(S_i^+ S_{i+2}^- + \text{H.c.}) \right\}.$$

Our spin-chain model with both nearest-neighbor and next-nearest-neighbor AFM interactions is bound to give rise to frustration. While the contribution from the z-z term can be easily accounted for through a shift in energy, the problematic terms are the raising/lowering parts, causing negative probability weights in the SSE-QMC algorithm. In order to circumvent this, we have thus used the following approximated version of the spin Hamiltonian in our QMC simulation:

$$H = J \sum_i^{N/3} \left[\left\{ S_{3i-1}^z S_{3i-2}^z + \frac{1}{2}(S_{3i-1}^+ S_{3i-2}^- + \text{H.c.}) \right\} \right.$$
$$\left. + \left\{ S_{3i}^z S_{3i-1}^z + \frac{1}{2}(S_{3i}^+ S_{3i-1}^- + \text{H.c.}) \right\} \right] + J' \sum_i^{N/3} S_{3i}^z S_{3i+1}^z$$
$$+ J_{nnn} \sum_i^N \left\{ S_i^z S_{i+2}^z + \frac{1}{2}(S_i^+ S_{i+2}^- + \text{H.c.}) \right\},$$

including only the Ising contribution for the J' interaction, with the J' interaction being much weaker than the dominant J_{nnn} interaction.

APPENDIX B: FINITE-SIZE SCALING

In order to ascertain the spin-gap values of the alternating-chain compound, one needs to carry out finite-size scaling analysis. For this purpose, we carried out additional calculations using a modified Lanczos technique [25]. Within this Lanczos method, we utilized a Gram-Schmidt orthonormalization technique which allowed us to calculate the lowest-energy gaps of the system. We cross-checked the validity of the Lanczos results and the exact diagonalization results for small system sizes.

Our finite-size scaling calculations carried out within the setup of periodic boundary conditions should exhibit odd-even oscillation which, however, should not affect the results at the asymptotic limit. In order to avoid such oscillation and to minimize the computational effort, we have restricted ourselves to the choice of only even-sized chains. Due to the computational expenses involved, we have also restricted ourselves to the choice of a few representative cases and a few representative sizes. We report here the results for the cases with $J = -J' = 26$ K, $J_{nnn} = 0$ K; $J = J' = 26$ K, $J_{nnn} = 0$ K; $J = -J' = 26$ K, $J_{nnn} = 78$ K; and $J = J' = 26$ K, $J_{nnn} = 78$ K. We chose the system size L to be an integral multiple of the periodicity of the spin lattice. It is important to note that the periodicity can differ depending on whether J_{nnn} is zero or nonzero and whether J and J' are the same or different, as elaborated below.

(i) For $J_{nnn} = 0$, $J = -J'$, the problem reduces to a spin chain with only nearest-neighbor interactions with the peri-
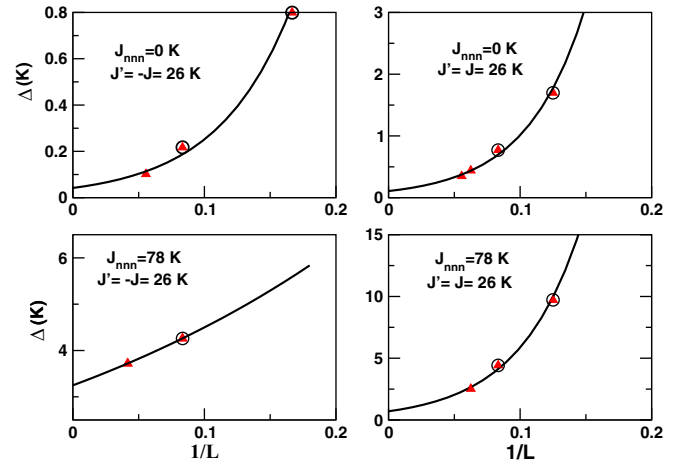

FIG. 7. Spin-gap values plotted as a function of inverse system size $(1/L)$. The data points shown as triangles were obtained from Lanczos calculations, while the data points shown as circles for small system sizes were obtained from exact diagonalization. The solid line is the fit through the data points to estimate the spin-gap value extrapolated to infinite system size.

odicity of the spin system being three lattice spacings. Thus preserving this symmetry of the Hamiltonian, one should use L values that are a multiple of 3. As we have considered only even lattice sizes, we considered L values of 6, 12, 18.

(ii) For $J_{nnn} = 0$, $J = J'$, the periodicity of the spin system is two lattice spacings. So any multiple of 2 can be used for L. In order for this case to be comparable with other considered cases, L values of 8, 12, 16, and 18 were chosen.

(iii) For a nonzero value of J_{nnn} (78 K in our case), $J = J'$, the periodicity is 4. The system sizes chosen are thus 8, 12, and 16.

(iv) For a nonzero value of J_{nnn} and $J = -J'$, the periodicity of the spin-lattice becomes 12. The system sizes chosen are thus 12 and 24.

The results are summarized in Fig. 7, where the calculated spin-gap values using the Lanczos technique as a function of inverse system size $(1/L)$ have been plotted. The exact diagonalization results for small system sizes are also shown, which are found to show excellent agreement with values obtained from the Lanczos technique. The spin-gap values extrapolated to infinite size give rise to vanishingly small values ($\leqslant 0.1$ K) for $J_{nnn} = 0$ K cases, while they show finite values ($\geqslant 1$ K) for $J_{nnn} = 78$ K cases. Specifically, we find that for $J = -J' = 26$ K, $J_{nnn} = 78$ K, the extrapolated spin gap is 3.25 K, thereby providing more confidence in the presence of spin gap in the discussed compound.

[1] A. Jain, S. Singh, and S. M. Yusuf, Phys. Rev. B **74**, 174419 (2006).

[2] D. Schmidiger, K. Yu. Povarov, S. Galeski, N. Reynolds, R. Bewley, T. Guidi, J. Ollivier, and A. Zheludev, Phys. Rev. Lett. **116**, 257203 (2016).

[3] M. Wang, M. Yi, S. Jin, H. Jiang, Y. Song, H. Luo, A. D. Christianson, C. de la Cruz, E. Bourret-Courchesne, D.-X. Yao, D. H. Lee, and R. J. Birgeneau, Phys. Rev. B **94**, 041111(R) (2016).

[4] K. Yonaga and N. Shibata, J. Phys. Soc. Jpn. **84**, 094706 (2015).

[5] I. Kimchi and A. Vishwanath, Phys. Rev. B **89**, 014414 (2014).

[6] E. A. Zvereva, M. A. Evstigneeva, V. B. Nalbandyan, O. A. Savelieva, S. A. Ibragimov, O. S. Volkova, L. I. Medvedeva, A. N. Vasiliev, R. Klingeler, and B. Buchner, Dalton Trans. **41**, 572 (2012).

[7] S.-Y. Zhang, W.-B. Guo, M. Yang, Y.-Y. Tang, M.-Y. Cui, N.-N. Wang, and Z.-Z. He, Dalton Trans. **44**, 20562 (2015).

[8] M. Kolb, R. Botet, and R. Jullien, J. Phys. A **16**, L673 (1983).

[9] H. A. Bethe, Z. Phys. **71**, 205 (1938).

[10] F. D. M. Haldane, Phys. Rev. Lett. **50**, 1153 (1983).

[11] K. M. Diederix, J. P. Groen, T. O. Klaassen, and N. J. Poulis, Phys. Rev. Lett. **41**, 1520 (1978).

[12] C. K. Majumdar and D. K. Ghosh, J. Math. Phys. **10**, 1388 (1969).

[13] L. Shvanskaya, O. Yakubovich, W. Massa, and A. Vasiliev, Acta Crystallogr., Sect. B **71**, 498 (2015).

[14] O. S. Volkova, L. V. Shvanskaya, E. A. Ovchenkov, E. A. Zvereva, A. S. Volkov, D. A. Chareev, K. Molla, B. Rahaman, T. Saha-Dasgupta, and A. N. Vasiliev, Inorg. Chem. **55**, 10692 (2016); K. V. Zakharov, E. A. Zvereva, M. M. Markina, M. I. Stratan, E. S. Kuznetsova, S. F. Dunaev, P. S. Berdonosov, V. A. Dolgikh, A. V. Olenev, S. A. Klimin, L. S. Mazaev, M. A. Kashchenko, Md. A. Ahmed, A. Banerjee, S. Bandyopadhyay, A. Iqbal, B. Rahaman, T. Saha-Dasgupta, and A. N. Vasiliev, Phys. Rev. B **94**, 054401 (2016); A. N. Vasiliev, O. S. Volkova,

E. A. Zvereva, A. V. Koshelev, V. S. Urusov, D. A. Chareev, V. I. Petkov, M. V. Sukhanov, B. Rahaman, and T. Saha-Dasgupta, *ibid.* **91**, 144406 (2015); P. S. Berdonosov, E. S. Kuznetsova, V. A. Dolgikh, A. V. Sobolev, I. A. Presniakov, A. V. Olenev, B. Rahaman, T. Saha-Dasgupta, K. V. Zakharov, E. A. Zvereva, O. S. Volkova, and A. N. Vasiliev, Inorg. Chem. **53**, 5830 (2014).

[15] W. Kohn and L. J. Sham, Phys. Rev. **140**, A1133 (1965).

[16] J. P. Perdew, K. Burke, and M. Ernzerhof, Phys. Rev. Lett. **77**, 3865 (1996).

[17] G. Kresse and J. Furthmuller, Phys. Rev. B **54**, 11169 (1996).

[18] O. K. Andersen and T. Saha-Dasgupta, Phys. Rev. B **62**, R16219(R) (2000).

[19] O. K. Andersen and O. Jepsen, Phys. Rev. Lett. **53**, 2571 (1984).

[20] V. I. Anisimov, I. V. Solovyev, M. A. Korotin, M. T. Czyżyk, and G. A. Sawatzky, Phys. Rev. B **48**, 16929 (1993).

[21] D. C. Johnston, J. W. Johnson, D. P. Goshorn, and A. J. Jacobson, Phys. Rev. B **35**, 219 (1987).

[22] A. W. Garrett, S. E. Nagler, D. A. Tennant, B. C. Sales, and T. Barnes, Phys. Rev. Lett. **79**, 745 (1997).

[23] S. Wessel, B. Normand, F. Mila, and A. Honecker, SciPost Phys. **3**, 005 (2017).

[24] J. C. Bonner and M. E. Fisher, Phys. Rev. **135**, A640 (1964).

[25] E. R. Gagliano, E. Dagotto, A. Moreo, and F. C. Alcaraz, Phys. Rev. B **34**, 1677 (1986).